Total electron-scattering cross sections from pyridine molecules in the energy range 1–200 eV

A. I. Lozano,[1,2] J. Jiménez,[1] F. Blanco,[3] and G. García[1,4,*]

[1]*Instituto de Física Fundamental, Consejo Superior de Investigaciones Científicas, 28006 Madrid, Spain*

[2]*Escuela de Doctorado de la UNED-Programa de Doctorado en Ciencias, 28015 Madrid, Spain*

[3]*Departamento de Física Atómica, Molecular y Nuclear, Universidad Complutense de Madrid, 28040 Madrid, Spain*

[4]*Centre for Medical Radiation Physics, University of Wollongong, NSW, Australia*

(Received 30 April 2018; published 17 July 2018)

We report on total electron-scattering cross sections from pyridine as measured with a magnetically confined electron-beam system for impact energies ranging from 1 to 200 eV, including measurements for energies below 10 eV. Reasonable agreement with previous measurements for energies above 10 eV has been found. Systematic errors arising from elastically and rotationally scattered electrons into the detector acceptance angle have been evaluated. Results are compared with available calculation both for the 10–200 eV and below 10 eV energy ranges. The evaluated data provided in this study will facilitate electron transport modeling in biologically relevant media.

DOI: 10.1103/PhysRevA.98.012709

I. INTRODUCTION

In the last decade, the need to understand microscopic radiation damage in biomolecular systems [1] has motivated numerous theoretical and experimental electron-scattering cross-section (CS) studies for biologically relevant molecules [2]. These data are needed to model radiation interactions with biological media [1] when accurate description of both energy deposition and induced molecular dissociation are required [3]. Pyridine has been considered a prototypical molecule for DNA bases and consequently it has received considerable attention in the last few years [4,5]. The total electron-scattering cross sections (TCSs) are an important parameter for checking the consistency of the collisional database available for a given molecular target. They represent the sum of the partial cross-section contributions from all scattering channels which are open at a given energy and therefore they are used as reference values to evaluate the completeness of a data set. In the case of pyridine, we have recently published experimental TCS values [6] for impact energies ranging from 10 to 1000 eV as measured with a double-spectrometer transmission-beam technique, together with an update of our previous Independent Atom Model with the Screening Corrected Additivity Rule (IAM-SCAR) calculation [5] by incorporating the effect of interferences in the elastic scattering cross sections (IAM-SCAR+I) [7]. Although those experimental results confirmed the reliability of the updated calculation by showing better agreement when interference terms are included, they are systematically lower than the calculated results, suggesting that new measurements with different techniques should be carried out to identify possible systematic errors. In addition, scattering resonances predicted by the available calculations below 10 eV [4,5] require experimental validation. Scattering of charged particles from polar molecules presents great difficulty both from the theoretical and experimental points of view. Even for one of the most well-studied molecules, water, great discrepancies remain between the total cross sections for low-energy electrons [8] and positrons [9] when results are compared between different theoretical and experimental sources. Pyridine possesses a relatively high permanent dipole moment (∼2.2 D [10]) and as such the lower-energy scattering is dominated by dipole interactions, therefore requiring greater detail when comparing results from different theoretical and experimental techniques to overcome this complication.

These considerations motivated the present experimental study, in which total electron-scattering cross sections from pyridine are measured using a state of the art magnetically confined transmission-beam technique [11]. This experimental system incorporates a nitrogen trap to cool the electron beam before entering the scattering region, providing accurate TCS measurements with random uncertainty limits within 5%.

The experimental technique and measurement procedures are described in Sec. II together with a detailed analysis of the possible uncertainty sources that may affect the present measurements. Results are presented in Sec. III and compared with available theoretical and experimental data. Finally, some concluding remarks are presented in Sec. IV.

II. EXPERIMENTAL SETUP AND MEASUREMENT PROCEDURE

The experimental system has been presented in detail in a previous article [11]; hence here we give only a brief description.

A schematic diagram of the experimental setup is shown in Fig. 1**.** The electron-beam line is divided into four sections: electron gun (EG), gas trap (GT), interface chamber (IC), scattering chamber (SC), and detector area (AD). The latter three are mutually separated by differential pumping and all sections of the experimental systems are surrounded by solenoids, generating axial magnetic fields of different intensities.

The primary electron beam is generated through thermionic emission by a tungsten filament, then extracted, collimated, and accelerated into the 60-mm-length nitrogen cooling trap.

*g.garcia@csic.es

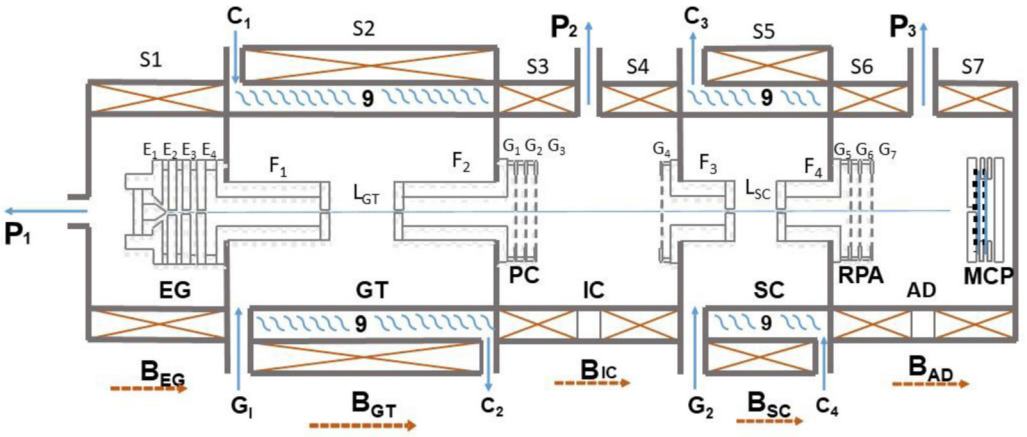

FIG. 1. Schematic diagram of the experimental setup: EG, electron gun; GT, gas trap; IC, interphase chamber; PC, pulse-controlling system; SC, scattering chamber; RPA, retarding potential analyzer; AD, detection area; MCP, microchannel plate detector; P_1, P_2, P_3, differential pumping system; B_{EG}, B_{GT}, B_{IC}, B_{SC}, B_{AD}, axial magnetic fields of the different chambers generated by the corresponding solenoids (S_1–S_7); C_1, C_2, C_3, C_4, water cooling system; G_1, G_2, gas inlet to the GT and SC, respectively. (See also text for further explanation.)

Here its energy spread is reduced down to about 200 meV by successive collisions with the cooling gas (N_2). The kinetic energy along the gas trap, around 7 eV, was optimized to balance the transmitted electron intensity and the effective cooling via vibrational and electronic excitation of the N_2 molecules. At the exit of the gas trap a three-grid system (PC) is used to pulse and control the electron beam. The axial magnetic field inside the gas trap (B_{GT}) was typically within 0.05–0.1 T. As described in Ref. [11] under these axial magnetic confinement conditions, any collision event in the GT chamber converts the expected scattering angle (θ) into a kinetic energy loss in the direction parallel to the beam (E_{II}), according to $E_{II} = E\cos^2\theta$, E being the incident kinetic energy. The scattering chamber (SC) has a similar geometry but it is 40 mm in length and the three-grid element at the exit constitutes a retarding potential energy analyzer (RPA). Pyridine is introduced into the SC through a leak valve and maintained to a constant pressure which was varied between 0 and 3 mTorr during the measurements. The target gas pressure was measured with an MKS Baratron (627B) capacitance manometer. Electrons transmitted through the RPA are finally detected by a two-stage microchannel plate operating in single-pulse-counting conditions. The kinetic energy of incident electrons in the SC is determined by $E = e|V_{GT} - V_{SC}|$, V_{GT} and V_{SC} being the potentials applied to the GT and SC, respectively. In this way the scattering energy is varied while still maintaining nitrogen cooling of the electron beam. The axial magnetic field inside the SC (B_{SC}) was 0.05–0.1 T in order to ensure magnetic confinement conditions [11]. The role of the remaining magnetic fields (B_{EG}, B_{IC}, and B_{AD}) is simply to guide the beam between chambers, and their intensities were optimized for each energy studied to maximize transmission while maintaining the energy resolution. The different stages are differentially pumped reaching background pressures of the order of 10^{-8} Torr and maintained below 10^{-6} Torr in the EG, IC, and AD stages during operation. Maximum GT and SC operating pressures were 60 and 3 mTorr, respectively.

Total cross sections are determined by the attenuation of the incident electron beam passing through a scattering chamber containing a well-known density of the molecular target according to the Lambert-Beer law:

$$I = I_0 e^{-n\sigma_T L}, \tag{1}$$

where I is the transmitted electron intensity, I_0 the initial intensity, n the molecular gas density, σ_T the total cross section, and L the interaction length. Assuming an ideal gas, this equation can be rewritten as

$$\ln\left(\frac{I}{I_0}\right) = -\frac{L\sigma_T}{kT}p, \tag{2}$$

where k is Boltzmann's constant, T is the absolute temperature, and p is the gas pressure. T is derived from $T = \sqrt{T_c T_m}$, where T_c and T_m are the temperature of the scattering chamber measured with a thermocouple and the Baratron gauge operating temperature. According to the above procedure, a semilogarithmic plot of Eq. (2) as a function of p can produce σ_T by simple slope (m) analysis, as follows:

$$\sigma_T = \frac{mkT}{L}. \tag{3}$$

In this way the electron transmission and attenuation as a function of pressure through a gas is able to provide TCS data.

Typical attenuation curves for different incident energies are shown in Fig. 2. As can be seen in the figure, single exponential functions can be used to fit all energies for the pressures used (1–3 mTorr), indicating multiple scattering processes are excluded from these measurements. Accurate values of the slope m can as such be determined to produce precise TCS data. For each incident electron energy, attenuation measurements were repeated at least five times to ensure that statistical uncertainties remained below 4%. Other random uncertainties are linked to the temperature measurement (within 1%, according to manufacturer's data) and the numerical fitting procedure (about 1%). By individually calculating these uncertainties for each incident energy, a random uncertainty maximum of 5% has been determined for the present measurements.

Possible systematic errors have been investigated in previous benchmarking measurements for molecular nitrogen [11].

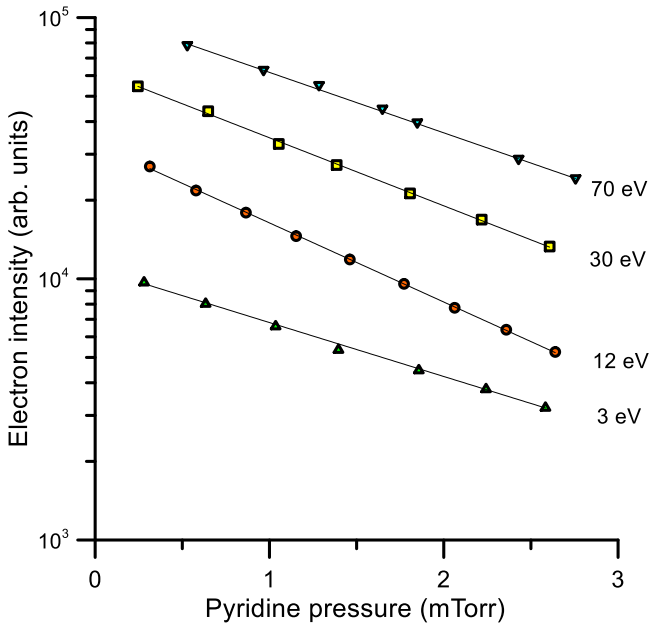

FIG. 2. Attenuation curves as a function of pyridine pressure for different impact energies.

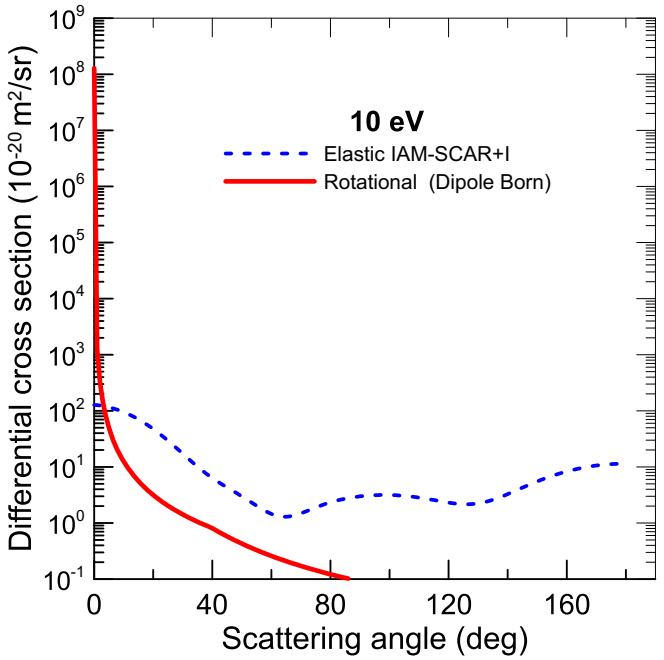

FIG. 3. Differential elastic cross section calculated with the present IAM-SCAR+I method and the differential rotational excitation cross sections derived from the Born approximation (see Ref. [5] for details).

Under the present experimental conditions space charge and multiple scattering effects are insignificant, evidenced by no dependence of the measured TCS values on electron current or gas pressure. In addition, the excellent agreement found for N_2 as compared with available reference data [12,13] indicates that the real interaction length coincides with the geometrical SC length and that the assumed magnetically confined conditions [11] are properly representing the scattering processes within the considered energy range. The magnetic confinement does produce an inherent systematic error in this technique, linked to the relationship between the angular resolution ($\Delta\theta$) and the energy resolution (ΔE), which is affecting the present measurements. As explained in Ref. [11], within the intense axial magnetic field, for elastic and rotational excitation collisions, the energy transferred to the target is negligible but the expected deflection (θ) of the scattered electron is converted into an energy loss (ΔE) in the direction of the axial magnetic field ($E_{\rm II} = E\cos^2\theta$). Obviously $\Delta E = E - E_{\rm II}$ and therefore the minimum scattering angle resolved ($\Delta\theta$) is linked to the energy resolution of the detector through the following expression (see Ref. [11] for details):

$$\Delta\theta = \arccos\sqrt{1 - \frac{\Delta E}{E}}. \tag{4}$$

Those electrons elastically or rotationally inelastically scattered into the $\Delta\theta$ angle are considered by the detector as unscattered, lowering the measured TCS. The magnitude of this systematic error, $\sigma(\Delta\theta)$, can be evaluated from theoretical data by integrating the calculated differential cross sections over the missing experimental angles:

$$\sigma(\Delta\theta) = 2\pi\left[\int_0^{\Delta\theta} \frac{d(\sigma_{\rm el}+\sigma_{\rm rot})}{d\Omega}\sin\,\theta d\theta + \int_{180-\Delta\theta}^{480} \frac{d(\sigma_{\rm el}+\sigma_{\rm rot})}{d\Omega}\sin\,\theta d\theta\right], \tag{5}$$

where $\sigma_{\rm el}$ and $\sigma_{\rm rot}$ represent the elastic and rotational cross sections, respectively. Depending on the target, vibrational excitation energies of the ground state may be lower than ΔE and so contribute to the $\sigma(\Delta\theta)$ term. Differential vibrational excitation cross sections from pyridine are not available in the literature but similar data for pyrimidine [3] indicate that the vibrational contribution to the angular resolution systematic error can be neglected. Calculated DCS can be used to evaluate the magnitude of the above systematic error. The main contribution to this uncertainty is due to the electron scattered into the experimental acceptance angles by rotational excitation processes. This situation is illustrated in Fig. 3, showing how for small scattering angles, below 1°, the rotational excitation DCS increases by more than five orders of magnitude when the scattering angle tends to zero for 10 eV incident electron energy. Note that more than 90% of this systematic error is due to the rotational excitation cross sections which are not discernible for most of the experiments and their calculated values mostly rely on the Born approximation [5].

III. RESULTS AND DISCUSSION

The present experimental TCSs with their absolute random uncertainty limits are shown in Table I. The energy resolutions and the corresponding angular resolutions [Eq. (4)] are also shown in this table for each incident energy. The latter can be used to determine the aforementioned systematic error by using the appropriate DCS values.

Experimental TCS data have been obtained by Traoré-Dubuis *et al.* [6] using a double-spectrometer transmission-beam technique. In the overlapping energy domain (13–174 eV), the present results are slightly higher than those of

TABLE I. Present experimental electron-scattering cross sections indicating their random uncertainty limits, the energy resolution, and the acceptance angle of the detector.

Energy (eV)	Total cross section (10^{-20} m^2)	Absolute random uncertainty limit (10^{-20} m^2)	Energy resolution (ΔE, in eV)	Acceptance angle ($\Delta\theta^\circ$)
1	36.8	0.87	0.22	27.9
1.2	39.2	0.57	0.23	25.9
1.5	35.4	1.1	0.22	22.5
1.7	31.5	0.67	0.23	21.6
2	30.4	1.2	0.23	19.8
2.3	34.7	1.5	0.23	18.4
2.6	37.1	1.4	0.23	17.3
2.8	38.7	1.3	0.23	16.6
3	40.3	1.5	0.20	14.9
3.2	37.8	1.0	0.21	14.8
3.5	34.6	1.2	0.22	14.5
3.7	38.7	1.2	0.20	13.4
4	44.1	1.9	0.23	13.8
4.2	49.1	2.1	0.23	13.5
4.4	51.3	1.1	0.23	13.2
4.6	53.6	2.0	0.23	12.9
4.8	51.7	1.2	0.23	12.6
5	49.6	1.6	0.23	12.4
5.2	45.2	1.9	0.23	12.1
5.5	47.8	1.3	0.22	11.5
5.8	50.2	1.5	0.22	11.2
6	50.1	2.4	0.22	11.0
6.5	53.7	0.90	0.22	10.6
7	57.8	2.2	0.22	10.2
7.5	55.1	1.6	0.21	9.63
8	55.7	2.3	0.20	9.10
8.5	60.4	2.6	0.20	8.82
9	58.7	2.0	0.22	8.99
9.5	58.8	1.1	0.20	8.34
10	60.3	2.2	0.19	7.92
11	58.9	2.9	0.24	8.49
12	55.1	1.7	0.23	7.96
13	51.1	1.7	0.27	8.29
14	55.6	1.7	0.19	6.69
15	54.4	2.6	0.19	6.46
16	52.3	1.6	0.20	6.42
17	51.4	0.79	0.20	6.23
20	50.9	2.4	0.22	6.02
25	50.9	1.7	0.22	5.38
30	48.2	1.6	0.22	4.91
40	45.9	1.4	0.22	4.25
50	44.3	1.3	0.20	3.63
70	39.9	0.91	0.22	3.21
90	37.7	0.61	0.18	2.56
100	36.2	1.2	0.24	2.81
150	29.3	0.65	0.24	2.29
200	24.3	0.87	0.24	1.98

Ref. [6] but the differences are less than 12%, so they are technically in agreement within the combined uncertainty limits. This difference cannot be explained by the better angular resolution (0.25° acceptance angle) used in Ref. [6] which would act in the opposite direction. We therefore could speculate that the possible pressure gradients mentioned in Ref. [6] are still affecting their results. An important motivation for measuring accurate TCSs is to check the consistency of the recently incorporated interference effects [7] with our IAM-SCAR calculation [5]. The significant permanent dipole moment (2.2 D [10]) of pyridine complicates this comparison at the elastic scattering level, especially for the lower energies where dipole rotational excitations are dominant. In addition, both interference effects and dipole interactions tend to preferentially scatter electrons in the forward direction, increasing the acceptance angle error of the experimental system. The experimental results are compared to literature data from three calculation methods: the integral elastic, inelastic, and total cross sections given by the IAM-SCAR+I [6] procedure and the rotationally summed integral elastic cross sections derived from the Schwinger multichannel (SMC) [4] and the *R*-matrix [5] methods. All three use the fixed nuclei representation; hence to include dipole interactions some corrections based on the Born approximation need to be implemented. In IAM-SCAR+I these take the form of approximated rotational cross sections, becoming the IAM-SCAR+I+R method. These approximated rotational excitation cross sections are in general less accurate than the respective original calculation methods and present some difficulties in reproducing the temperature-dependent initial rotational state distributions of the experimental targets. Keeping in mind these considerations a comparison between the experimental and theoretical results is plotted in Fig. 4.

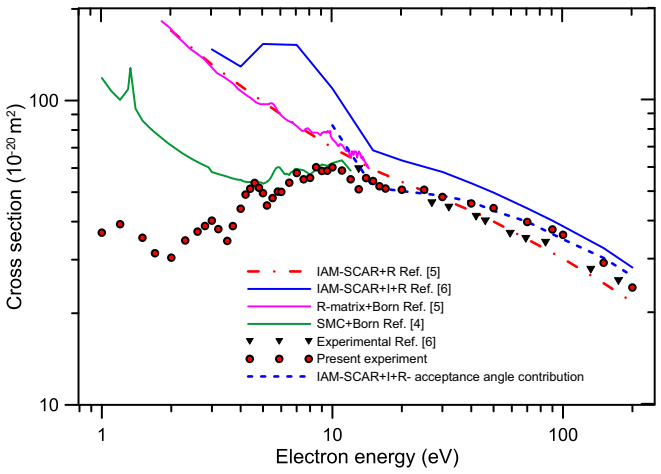

FIG. 4. Rotationally summed integral elastic cross sections calculated in Refs. [4,5], total electron-scattering cross sections calculated in Refs. [5,6] with and without acceptance angle corrections, and present electron-scattering cross-section measurements (see also legend for symbols and text for details).

Comparing the present experimental TCSs with those calculated with our IAM-SCAR+I+R [6] method, the theoretical values are generally higher than the experimental by 10%–25% for impact energies above 10 eV. Below 10 eV the IAM-SCAR approximation [14,15] does not apply and we can only expect a qualitative estimate. For this reason, we are not including in this comparison the IAM-SCAR data below 10 eV. In this energy domain, a more sophisticated description of the molecular wave functions and the scattering equation is required to obtain

suitable cross-section values and account for resonances. If we compare our experimental results with the Born corrected SMC calculation from Ref. [4], the experimental data are in general lower in magnitude. As the calculations include rotational excitation and the measurements do not account for them, comparison between the absolute values does not make sense but the position of the resonances can be discussed. Note that below 2.5 eV, they agree well on the position of a low-lying resonance. Earlier theoretical studies from Mašín *et al.* [16] predicted four π^* shape resonances in electron collisions with diazines. However, in the case of pyridine (azine) Sieradzka *et al.* [5] only found three π^* resonances. The SMC calculation for pyridine from Ref. [4], in the energy range considered in this study, identifies resonances at 1. 33 eV which can be classified as $^2A_2$ (see Refs. [4,5]) and another, $^2B_1$, at 5.80 eV.

Our experimental results show a resonance at 1.2 ± 0.2 eV, which is in agreement with the $^2A_2$ calculated by Barbosa *et al.* [4]. We can also distinguish a resonance at 4.6 ± 0.2 eV which is about 1.3 eV lower in energy than the $^2B_1$ given in Ref. [4], but in perfect agreement with the 4.58 eV shape resonance experimentally identified by Nenner and Schultz [17]. In addition, Modelli and Burrow [18] studying temporary anion formation in pyridine with an electron-transmission technique found this resonance at 4.48 eV, in agreement with the present result within experimental uncertainty. The *R*-matrix calculation from Ref. [5] also predicts well the position of the $^2A_2$ resonance at 1.07 eV, but gives an energy position for the $^2B_1$ which is 16% higher in energy than the present experimental value.

The R-matrix integral elastic cross sections (IECSs) [5] with the equivalent SMC results [4] (both rotationally summed and Born corrected) clearly differ. Initial discrepancies between the non-Born-corrected results were discussed in Ref. [5]. These were attributed to the different basis sets used by the two methods and the treatment of the long-range polarization interaction, which is not considered in the external *R*-matrix sphere [5]. The Born correction procedure to include the higher-order partial waves in the calculation was essentially the same in both methods, based on the original formulation of Lucchese and Gianturco [19]. However, the *R*-matrix [5] IECS values are about a factor of 2 higher in magnitude than the SMC for impact energies below 5 eV. As mentioned above, at energies below 10 eV, where the independent atom approximation fails, it does not make sense to compare experiment with the IAM-SCAR+I+R calculation. However, it is interesting to note the different method with which the latter incorporates rotational excitations. While *R*-matrix and SMC methods consider the target molecule in its ground rotational state before the collision, the IAM-SCAR+I+R assumes a thermal distribution of the initial *J*-rotational states [20] accessible at room temperature and then calculates $\Delta J = \pm 1$ transitions within the framework of the Born approximation [21], including the Dickinson correction [22] for large scattering angles. The ionization energy of pyridine is 9.51 eV [23]. For energies above 10 eV, the reliability of this representation is shown by the good agreement in Fig. 4 between the present experimental data and the IAM-SCAR+I+R calculation when the aforementioned $\sigma(\Delta\theta)$ correction, which is mainly due to rotational excitations, is subtracted from the calculated TCSs. The effect of this subtraction within the energy range from 10 to 200 eV is lowering the calculated TCSs from 25% to 6%, respectively.

In addition, between 2.2 and 3.5 eV we obtained a resonant-type cross-section increase, not seen in either calculation, with a local maximum at 3.0 ± 0.2 eV. This may be attributed to the excitation of an inelastic channel not included in the respective calculations. Considering the experimental energy loss study of Walker *et al.* [24], no electronic excitation peak appears around that energy. We can therefore assign this peak to the vibrational excitation of the ground state. No data were found in the literature on vibrational excitation of pyridine by electron impact but a compilation of vibrational excitation cross sections of pyrimidine [25] exists. This showed that vibrational excitations of the ground state for this molecule present a prominent maximum in cross section of about 10×10^{-20} m^2 at a collision energy of 4 eV, which is compatible with the increase on the cross section we measured for pyridine around 3 eV. The next cross-section increase begins at 3.7 eV reaching a local maximum at 4.6 ± 0.2 eV; this has been identified as the $^2B_1\,\pi^*$ resonance described in Refs. [16,17]. Further local maxima of the experimental TCS appear at 7, 8.5, and 10 eV, corresponding to two electronic excitation levels and ionization, respectively. The 7.0 ± 0.2 eV inelastic feature is consistent with the position of the strongest optical band, with a maximum energy at 7.22 eV [26], which has been attributed to the excitation of the $^1B_2 + {}^1A_1$ states of pyridine. The 8.5 ± 0.2 eV structure is seen in Ref. [24], with a maximum energy value at 8.24 eV, and in the higher impact energy absorption measurements performed by Jonsson and Lindholm [27], which are attributed to valence state excitations. Finally, the broad structure around 10 eV can be attributed to excited Rydberg states together with ionizing transitions to continuum states. These electronic excitation and ionisation structures are not reproduced by the rotationally summed elastic scattering SMC calculation, and their lower result can reasonably be ascribed to these contributions in the measured TCS.

IV. CONCLUDING REMARKS

Total electron-scattering cross sections from pyridine have been measured in the energy range 1–200 eV by using a magnetically confined transmission-beam technique. Random uncertainty limits are less than 5%. Systematic errors arising from the scattering information missing within the detector's acceptance angle have been discussed and detailed information on the energy and angular resolution of the present measurements is detailed in order to allow a proper estimation of their magnitude. For energies above 10 eV present measurements show a reasonable agreement, within the combined uncertainty limits, with our previous results [6], measured with a double-spectrometer attenuation-beam system. By subtracting the calculated magnitude of this systematic error from our theoretical IAM-SCAR+I+R total cross sections, we obtained a set of "corrected values" which have been found to be in excellent agreement with our experimental data above 10 eV. Since the main contribution to this correction comes from the rotational excitation cross section we can conclude that our free rotating electric dipole representation based on the Born approximation to calculate dipole-induced rotational

excitation cross sections reproduces the present experimental conditions well in the energy range 10–200 eV. This also indicates that interference effects affecting mainly the forward elastic scattering amplitudes [7] should be considered by independent atom calculations to properly agree with accurate integral cross-section measurements. Below 10 eV we have found reasonable agreement with the SMC [4] calculation in terms of resonance positions corresponding to the trapping of an electron in two of the three π^* orbitals of pyridine at 1.2–1.6 and 4–5.5 eV, respectively. A feature at 3 eV has also been attributed to the ground-state vibrational excitation cross sections, with a maximum contribution to the TCS of about 10×10^{-20} m^2. The R-matrix calculation [5] seems to be less accurate in finding the position of the shape resonances. Other inelastic features have been identified as electronic excitation and ionization transitions consistent with early electron spectroscopy studies [24,26,27]. These cross sections for pyridine facilitate further electron transport simulations in biologically relevant media.

ACKNOWLEDGMENTS

This experimental study has been partially supported by the Spanish Ministerio de Ciencia, Innovación y Universidades (Project No. FIS 2016-80440) and the FP7 ITN ARGENT Project (Project No. 608163). A.I.L. also acknowledges the "Garantía Juvenil" grant programme from Ministerio de Ciencia, Innovación y Universidades. J.J. acknowledges support from the Master's Programme of the Universidad Complutense de Madrid.

[1] *Radiation Damage in Biomolecular Systems*, edited by G. García Gómez-Tejedor and M. C. Fuss (Springer, London, 2012).
[2] I. Baccarelli, I. Bald, F. A. Gianturco, E. Illemberger, and J. Kopyra, Phys. Rep. **508**, 1 (2011).
[3] M. C. Fuss, L. Ellis-Gibbings, D. B. Jones, M. J. Brunger, F. Blanco, A. Muñoz, P. Limão-Vieira, and G. García, J. Appl. Phys. **117**, 214701 (2015).
[4] A. S. Barbosa, D. F. Pastega, and M. H. F. Bettega, Phys. Rev. A **88**, 022705 (2013).
[5] A. Sieradzka, F. Blanco, M. C. Fuss, Z. Mašín, J. D. Gorfinkiel, and G. García, J. Phys. Chem. A **118**, 6657 (2014).
[6] A. Traoré Dubuis, F. Costa, F. Ferreira da Silva, P. Limão-Vieira, J. C. Oller, F. Blanco, and G. García, Chem. Phys. Lett. **699**, 182 (2018).
[7] F. Blanco, L. Ellis-Gibbings, and G. García, Chem. Phys. Lett. **645**, 71 (2016).
[8] A. Muñoz, J. C. Oller, F. Blanco, J. D. Gorfinkiel, P. Limao-Vieira, and G. García, Phys. Rev. A **76**, 052707 (2007).
[9] W. Tattersall, L. Chiari, J. R. Machacek, E. Anderson, R. D. White, M. J. Brunger, S. J. Buckman, G. Garcia, F. Blanco, and J. P. Sullivan, J. Chem. Phys. **140**, 044320 (2014).
[10] *NIST Standard Reference Database No. 101*, edited by R. D. Johnson III (U.S. Department of Commerce, Washington, DC, 2018); http://cccbdb.nist.gov/.
[11] A. I. Lozano, J. C. Oller, K. Krupa, F. Ferreira da Silva, P. Limão-Vieira, F. Blanco, A. Muñoz, R. Colmenares, and G. García, Rev. Sci. Instrum. **89**, 063105 (2018).
[12] Y. Itikawa, J. Phys. Chem. Ref. Data **35**, 31 (2006).
[13] C. Szmytkowski and K. Maciag, Phys. Scr. **54**, 271 (1996).
[14] F. Blanco and G. García, Phys. Rev. A **67**, 022701 (2003).
[15] F. Blanco and G. García, Phys. Lett. A **317**, 458 (2003).
[16] Z. Mašín and J. Gorfinkiel, J. Chem. Phys. **137**, 204312 (2012).
[17] I. Nenner and G. J. Schultz, J. Chem. Phys. **62**, 1747 (1975).
[18] A. Modelli and P. Burrow, J. Electron Spectrosc. Relat. Phenom. **32**, 263 (1983).
[19] R. R. Lucchese and F. A. Gianturco, Int. Rev. Phys. Chem. **15**, 429 (1996).
[20] A. G. Sanz, M. C. Fuss, F. Blanco, F. Sebastianelli, F. A. Gianturco, and G. García, J. Chem. Phys. **137**, 124103 (2012).
[21] A. Jain, J. Phys. B **21**, 905 (1988).
[22] A. S. Dickinson, J. Phys. B **10**, 967 (1977).
[23] *NIST Chemistry WebBook* (U.S. Department of Commerce, Washington, DC, 2017); https://webbook.nist.gov/chemistry/.
[24] I. C. Walker, M. H. Palmer, and A. Hopkirk, Chem. Phys. **141**, 365, (1989).
[25] M. J. Brunger, K. Ratnavelu, S. J. Buckman, D. B. Jones, A. Muñoz, F. Blanco, and G. García, Eur. Phys. J. D **70**, 46 (2016).
[26] A. Bolovinos, P. Tsekeris, J. Philis, E. Pantos, and G. Anditsopoulos, J. Mol. Spectrosc. **103**, 240 (1984).
[27] B. O. Jonsson and E. Lindholm, Int. J. Mass Spectrom. Ion Phys. **3**, 385 (1969).